# Effect of high-temperature exposure on matrix microstructure and fibre-matrix interface of all-oxide ceramic matrix composites

DLR IB 334-02/17

DLR

# Document properties

| | |
|---|---|
| Title | Effect of high-temperature exposure on matrix microstructure and fibre-matrix interface of all-oxide ceramic matrix composites |
| Authors | Henning Richter, Liudmila Chernova |
| | henning.richter@dlr.de, liudmila.chernova@dlr.de |
| Institute | Institute of Materials Research |
| Date | 24.05.2017 |

# Contents

# Abstract

The effects of extended high-temperature exposure on the microstructure of an all-oxide ceramic matrix composite consisting of Nextel™ 610 fibres and a highly porous alumina matrix phase are outlined in this report. The microstructure evolution of the porous matrix phase after high-temperature exposure was investigated by scanning electron microscopy and bulk density measurements. The variation of the fibre-matrix interface was analysed by determining the length fractions of matrix particle segments sintered to the fibre contour from polished cross-sections. Specimens with both uni- and bidirectional fibre orientation were investigated to account for varying constraints on matrix densification during high-temperature exposure.

# 1. Introduction

The fracture toughness of ceramic matrix composites (CMCs) critically depends on a sufficiently weak fibre-matrix bonding, which enables crack deflection and fibre-matrix separation during loading in order to advantageously use the comparatively high strain-to-failure of the ceramic fibres [1, 2, 3]. Weak fibre-matrix bonding is commonly obtained either by applying thin or fugitive fibre coatings [4, 5] or by using porous matrices [6, 7]. The underlying intent of both approaches is to prevent a matrix crack from penetrating the fibres by manipulating the crack path either right at the fibre-matrix interface or in the porous matrix interphase immediately surrounding the fibres.

With regard to the fact that CMC components are typically used at high temperatures in severe environments, the long-term stability of the fibre-matrix interface or interphase plays a critical role in their mechanical performance: carbon fibre-matrix interfaces, which are commonly used with non-oxide CMCs, are known to suffer from oxidation [8, 9], while porous oxide matrix interphases, which form due to partial, short-time sintering of the green bodies, are prone to resintering and densification during extended use at high temperatures [10]. The detrimental effect of both oxidation and matrix densification on the mechanical strength of non-oxide and all-oxide CMCs has been demonstrated experimentally [9, 11, 12, 13].

Against this background, the aim of the present report is to illustrate the effects of extended high-temperature exposure on the microstructure of an all-oxide CMC consisting of Nextel™ 610 fibres [14] embedded in a highly porous alumina matrix phase [15, 16]. The microstructure evolution of the porous matrix phase after different exposure times was investigated by scanning electron microscopy and quantified in terms of the increase in matrix bulk density. Furthermore, the variation of the fibre-matrix interface was analysed by determining the length fractions of matrix particle segments sintered to the fibre contour from polished cross-sections of thermally exposed specimens. Specimens with both uni- and bidirectional fibre orientation were investigated to account for constraints on matrix shrinkage imposed by the embedded fibres during high-temperature exposure.

# 2. Experimental

## 2.1. Specimen preparation

Three generic specimen types, namely an unreinforced matrix cast (subsequently referred to as ‘pure matrix’ or ‘PM’), a unidirectional impregnated fibre bundle (‘mini-composite’ or ‘MC’) and a bidirectional ceramic matrix composite with $\alpha = \pm 45°$ fibre orientation (‘laminate’ or ‘LAM’), were investigated.

Five pure matrix specimens were obtained by pouring an aqueous slurry of $\alpha$-$Al_2O_3$ particles with an average particle size of approximately 200 nm, prepared from PURAL® boehmite powder [17], into a gypsum mould [15, 16]. The matrix specimens were dried and pre-sintered in air for one hour at a temperature of 800 °C in order to determine the initial matrix density close to the green state.

Finally, these specimens were sintered in air for one hour at 1300 °C.

The specimens containing fibres were manufactured by filament winding, using a continuous Nextel™ 610 fibre roving with 3000 denier linear mass density [14], which had been de-sized and infiltrated with the alumina matrix slurry [15, 16]. Three mini-composite specimens were prepared by manually removing infiltrated roving sections prior to the filament winding process, and three different-sized laminate specimens were cut from a filament wound cylinder. All specimens were pre-dried and sintered in air for one hour at a temperature of 1300 °C. After sintering, the matrix phase of the specimens exhibits an alumina content of more than 99.8 wt%.

The specimens' fibre volume fraction $\varphi$ was determined either by counting the individual fibres on cross-sectional images of the mini-composite specimens and approximating the overall fibre volume for the given specimen length and an average fibre diameter of 11.8 µm or by recording the dry mass of the roving section used during filament winding of the composite cylinder and computing the overall fibre volume with the known fibre density.

## 2.2. High-temperature exposure

All specimens were thermally treated at 1300 °C in air for up to $t = 100$ hours in a laboratory muffle furnace. Each thermal treatment consisted of three stages: the preheating stage using heat-up rates of 10 °C/min up to a temperature of 700 °C and 3.5 °C/min from 700 °C to 1300 °C, the time $t$ at 1300 °C, and the cooling stage. The specimens were not taken out of the furnace until they had attained room temperature to avoid damage due to thermal shock.

## 2.3. Density measurements

After each thermal treatment, bulk and skeletal density of the specimens were determined based on Archimedes' principle: the dry weight $m_{\mathrm{dry}}$ was determined after heating the specimens to 100 °C for one hour to remove any remaining moisture from the pores. The immersed weight $m_{\mathrm{im}}$ was measured after saturating the specimens in purified water (with temperature-dependent density $\rho_{\mathrm{fl}}$) using a sealed container attached to a vacuum pump. The weight $m_{\mathrm{sat}}$ of the water-saturated specimens in air was determined after removing water drops from the specimens' surface with a wet cloth. Each specimen was weighed three times in the dry, immersed, and water-saturated state, and the respective arithmetic means were used for the calculation of the specimen's bulk and skeletal density.

## 2.4. Microstructure investigation

After $t = 1$ h, 50 h and 100 h, polished cross-sections of thermally treated specimens were investigated by scanning electron microscopy. The specimens were infiltrated with a low-viscous epoxy resin prior to cutting and polishing. For each specimen, high-magnification images of five randomly selected fibres were taken to detect variations in the microstructure of the fibre-matrix interfacial region.

# 3. Analytical

## 3.1. Matrix density determination

For the porous CMC specimens, bulk density $\rho$ is given by the relation

$$\rho = \frac{m_\mathrm{f} + m_\mathrm{m}}{V_\mathrm{f} + V_\mathrm{m} + V_\mathrm{p}} = \frac{m_\mathrm{dry}\,\rho_\mathrm{fl}}{m_\mathrm{sat} - m_\mathrm{im}}, \tag{3-1}$$

where $m_\mathrm{f}$ and $m_\mathrm{m}$ denote the mass of the fibres and the matrix phase, $V_\mathrm{f}$ and $V_\mathrm{m}$ are the fibre and matrix volume including closed pores, respectively, and $V_\mathrm{p}$ is the total volume of open, interconnected pores in the matrix phase. The bulk density $\rho_\mathrm{m}$ of the porous matrix phase can be obtained from Eq. (3-1) as

$$\rho_\mathrm{m} = \frac{m_\mathrm{m}}{V_\mathrm{m} + V_\mathrm{p}} = \frac{\rho - \rho_{\mathrm{f}_0}\,\varphi}{1 - \varphi}, \tag{3-2}$$

assuming that the fibres with skeletal density $\rho_{\mathrm{f}_0} = 3.9$ g/cm$^3$ [14] contain no open pores. The fibre volume fraction $\varphi$ of the investigated specimens, which is defined as

$$\varphi = \frac{V_\mathrm{f}}{V_\mathrm{f} + V_\mathrm{m} + V_\mathrm{p}}, \tag{3-3}$$

was recomputed after each thermal treatment to account for sintering-induced changes in matrix volume. For pure matrix specimens with $\varphi$ = 0, matrix bulk density corresponds to overall bulk density $\rho_\mathrm{m} = \rho$.

The skeletal solid density $\rho_0$ of specimens containing fibres is given by

$$\rho_0 = \frac{m_\mathrm{f} + m_\mathrm{m}}{V_\mathrm{f} + V_\mathrm{m}} = \frac{m_\mathrm{dry}\,\rho_\mathrm{fl}}{m_\mathrm{dry} - m_\mathrm{im}}, \tag{3-4}$$

from which the matrix skeletal density $\rho_{\mathrm{m}_0}$ is obtained as

$$\rho_{\mathrm{m}_0} = \rho_0 + \left(\rho_0 - \rho_{\mathrm{f}_0}\right)\frac{V_\mathrm{f}}{V_\mathrm{m}}. \tag{3-5}$$

For pure matrix specimens with $V_\mathrm{f}$ = 0, matrix skeletal density reads $\rho_{\mathrm{m}_0} = \rho_0$.

## 3.2. Fibre-matrix interface characterisation

On each cross-sectional image of the fibre-matrix interfacial region, the lengths $l_\mathrm{s}$ of the matrix particle segments sintered to the fibre contour right at the investigated cross-section were digitally evaluated using the ImageJ image analysis toolbox [18]. The sum of all these lengths was related to the fibre perimeter $L$, which was found on the cross-sectional image by fitting an ellipse to the

fibre contour and computing the ellipse's perimeter, in order to determine the length fraction

$$\delta = \frac{\sum l_s}{L} \tag{3-6}$$

of sintered particle segments.

# 4. Results

## 4.1. Matrix densification

The variation in the ratio of matrix bulk density to matrix skeletal density $\rho_m/\rho_{m_0}$ over time $t$ of thermal exposure to 1300 °C is plotted in Fig. 4-1. The five pure matrix (PM) specimens had a mean bulk density of 2.48 g/cm$^3$ after pre-sintering for one hour at 800 °C. They exhibit a pronounced increase in the ratio $\rho_m/\rho_{m_0}$ from, on average, 0.63 after sintering for one hour at 1300 °C to 0.70 after ten hours and 0.83 after 100 hours, cf. Fig. 4-1(a). It is assumed that the observed ratio $\rho_m/\rho_{m_0}$ is not significantly affected by the presence of closed pores, because the transition from open to fully closed porosity in specimens prepared from alumina slurry is reported to occur at $\rho_m/\rho_{m_0} > 0.9$ [19].

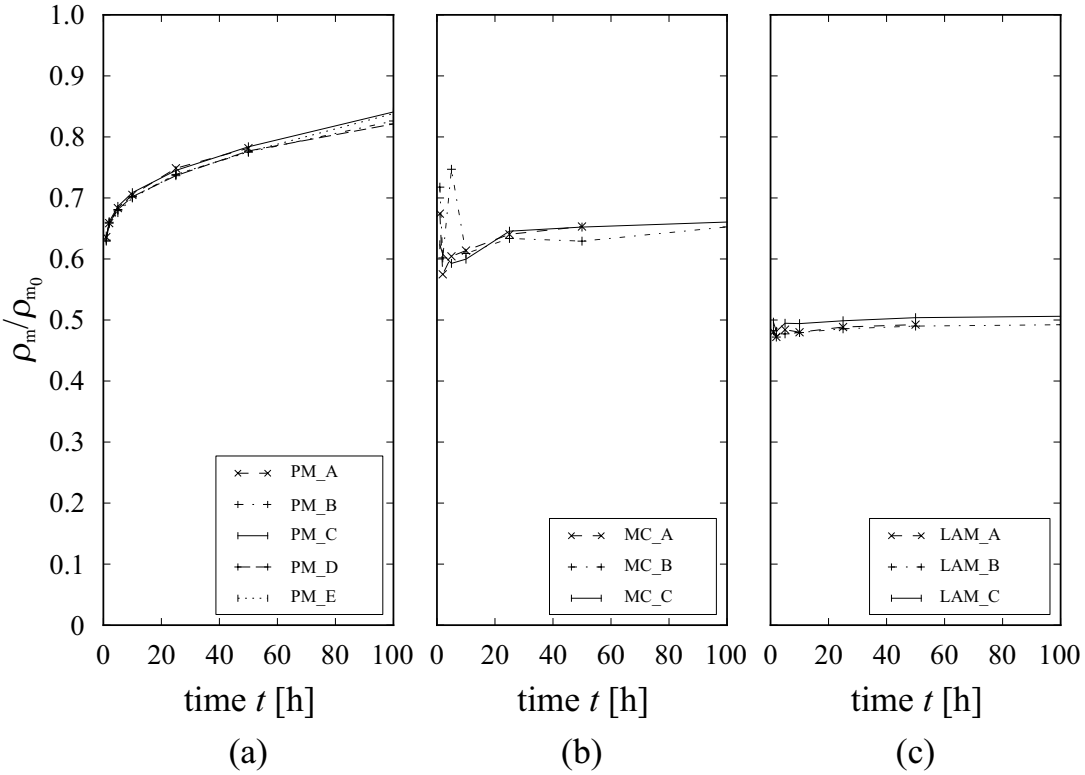


4-1 Increase in the ratio of matrix bulk density to matrix skeletal density $\rho_m/\rho_{m_0}$ over time $t$ of thermal exposure to a temperature of 1300 °C for pure matrix (a), unidirectional mini-composite (b) and bidirectional laminate specimens with $\alpha = \pm 45°$ fibre orientation (c).

Unidirectional mini-composites (MC) show an initial increase from a mean ratio $\rho_m/\rho_{m_0}$ of approximately 0.60 after two hours to 0.64 after 25 hours at 1300 °C, which is mainly attributed to the radial shrinkage of the matrix phase. For extended times $t$, the increase in the ratio $\rho_m/\rho_{m_0}$ is only moderate, reaching finally 0.66 on average after 100 hours, cf. Fig. 4-1(b). The unexpectedly high values of the ratio $\rho_m/\rho_{m_0}$ for mini-composite specimens MC_A and MC_B after one hour and for specimen MC_B after five hours at 1300 °C were caused by failures of the vacuum system while saturating the specimens with water, leading to erroneously low values for the weight of the water-saturated specimens and, consequently, very high values for the matrix bulk density.

Bidirectional laminate (LAM) specimens with $\alpha = \pm 45°$ fibre orientation exhibit a comparatively low initial matrix bulk density, cf. Fig. 4-1(c), which results from the presence of processing-induced macropores between the wound fibre layers and at roving intersections. These specimens show a very modest increase in the ratio $\rho_m/\rho_{m_0}$ from, on average, 0.49 after one hour to approximately 0.50 after 100 hours at 1300 °C.

## 4.2. Matrix microstructure evolution

The observed differences in matrix densification are echoed in the evolution of the matrix microstructure of the corresponding specimens. Cross-sectional images of pure matrix specimens and the inter-fibre matrix microstructure of specimens containing fibres after different times of thermal exposure are shown in Fig. 4-2.

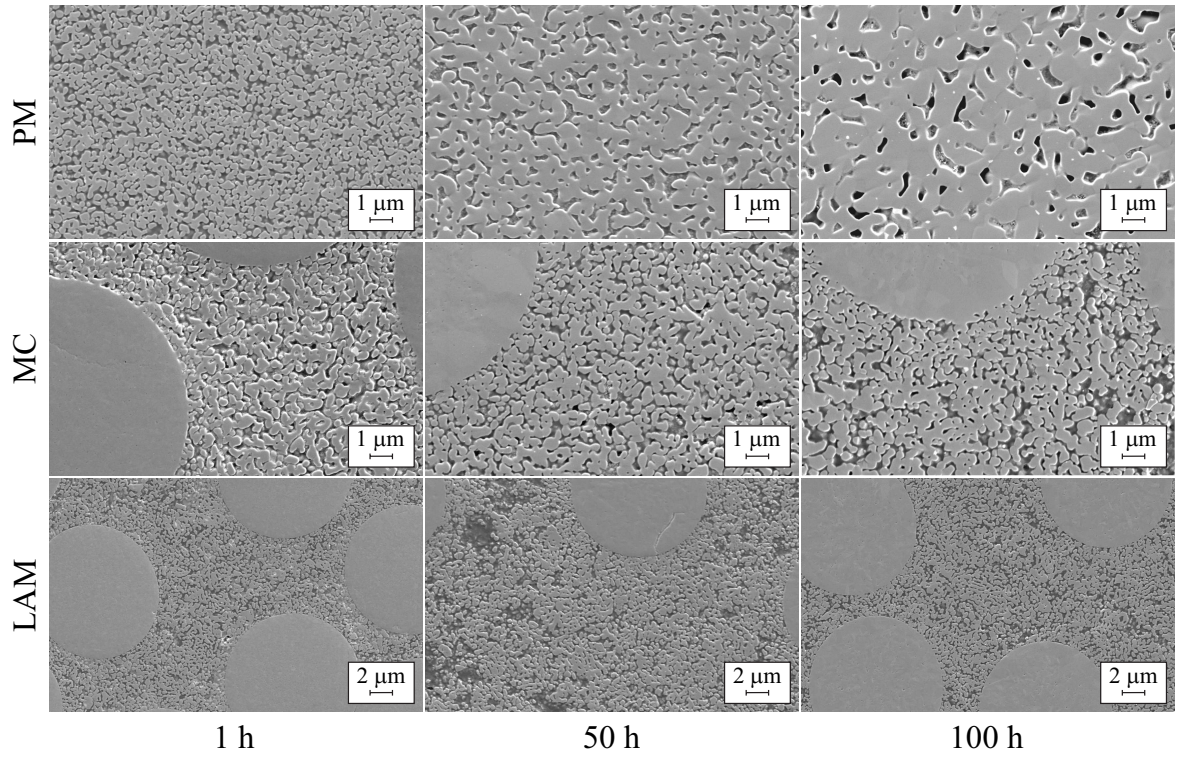


4-2 Scanning electron microscopic images of the (inter-fibre) matrix microstructure of randomly selected pure matrix (PM), mini-composite (MC) and laminate (LAM) specimens after thermal exposure to 1300 °C for different times $t$.

Pure matrix specimens exhibit mainly fine-scale porosity. During thermal exposure, unhindered matrix shrinkage leads to an initially rapid increase in bulk density and grain size. The rate of increase in bulk density is, however, regressive, as the driving force for solid-state sintering diminishes with increasing diffusion distance in larger grains [20].

On the inter-fibre matrix regions of mini-composites and laminate specimens, pronounced matrix grain growth after extended exposure to 1300 °C was not observed (Fig. 4-2). However, grain growth in the fibres occurs, as can be seen on the images of fibre cross-sections plotted in Fig. 4-3, which is expected to impair fibre strength [21].

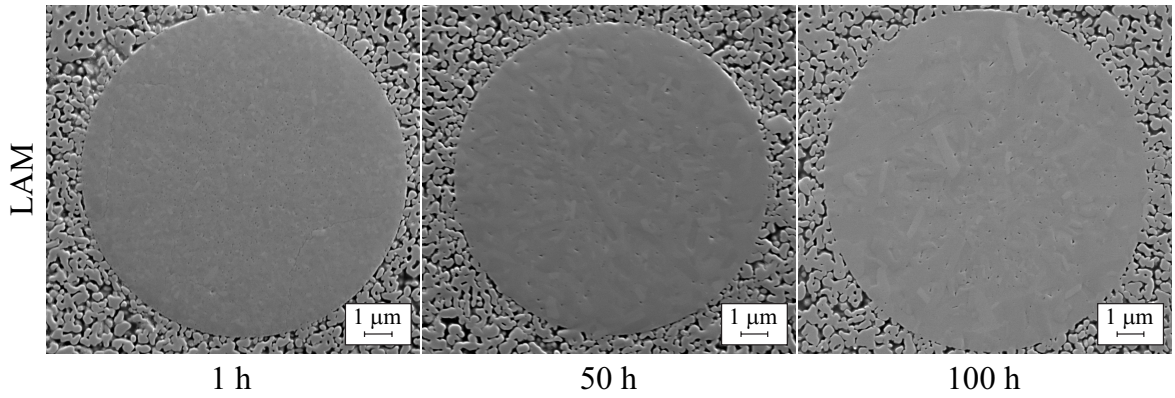


4-3 Scanning electron microscopic images of fibre cross-sections in laminate (LAM) specimens after thermal exposure to 1300 °C for different times $t$.

## 4.3. Fibre-matrix interface

The length fractions $\delta$ of particle segments sintered to the fibre contours in both mini-composite (MC) and laminate (LAM) specimens after different times of thermal exposure to 1300 °C are plotted in Fig. 4-4. On each specimen, five randomly selected fibres were evaluated, as shown in Fig. 4-4.

Due to the fact that the lengths $l_s$ of sintered matrix particle segments were determined manually on digital images of fibre cross-sections using the ImageJ toolbox, the length fraction $\delta$ of sintered particle segments is principally a qualitative variable. The length fractions of the individual specimens exhibit large scatter, however, the arithmetic means tend to increase with longer times of thermal exposure. After one hour at 1300 °C, the mean length fractions of sintered particles of both mini-composite and laminate specimens are similar, reading 37.4% for mini-composite and 35.1% for laminate specimens. After 100 hours at 1300 °C, the mean length fractions have increased to 50.8% for mini-composite and to 44.5% for laminate specimens.

The observed increase in mean length fractions $\delta$ is attributed to an augmentation of the lengths $l_s$ of sintered matrix particle segments for extended times $t$, as illustrated by the histograms of the lengths $l_s$ shown in Fig. 4-5. To generate the histograms, the lengths $l_s$ measured on all five specimens for each time $t$ of thermal exposure were treated as combined set of data, respectively.

The overall increase in lengths $l_s$ of sintered matrix particle segments with time $t$ becomes apparent from the corresponding box plots shown on the left of the histograms in Fig. 4-5: each box represents binned data that fall between the first and third quartile of the distribution of lengths

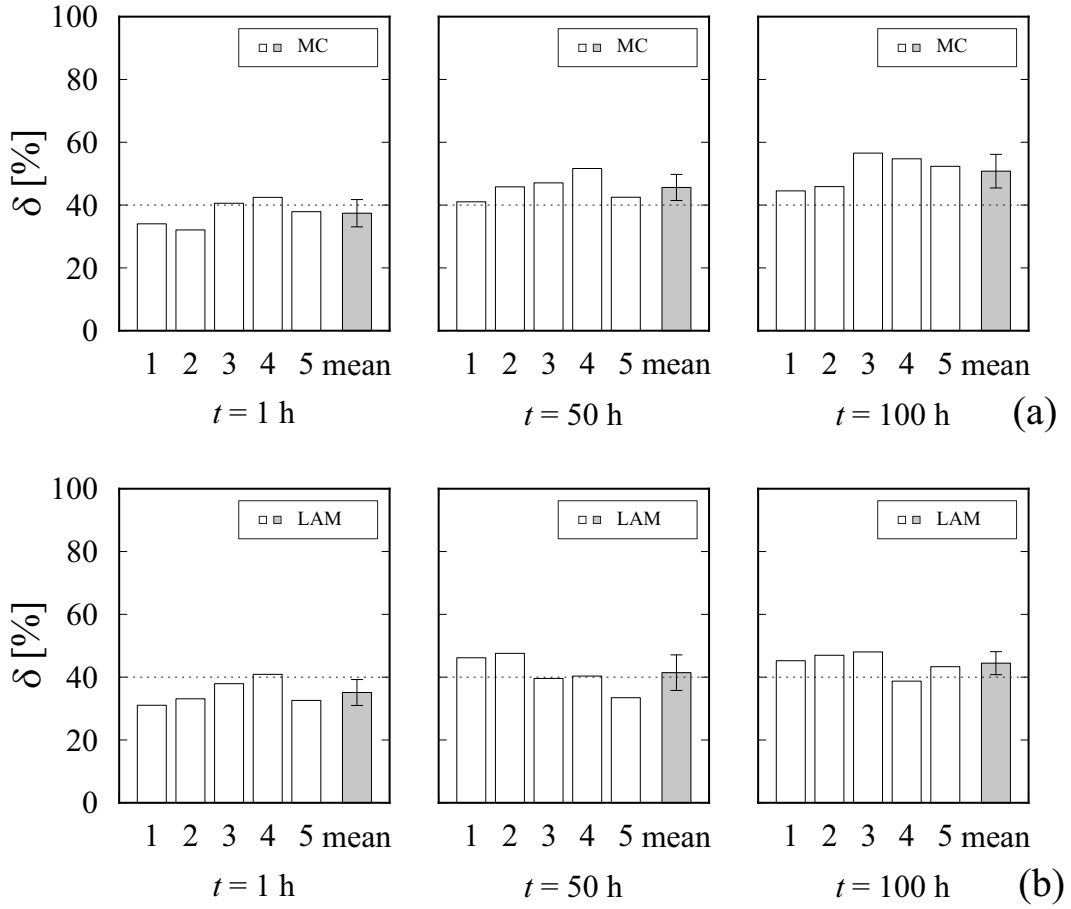


4-4 Length fractions $\delta$ of sintered particle segments at five random fibre cross-sections in mini-composite (a) and laminate specimens (b) after thermal exposure to 1300 °C for different times $t$. The shaded bars correspond to the arithmetic mean, the error bars represent the standard deviation of each data sample.

$l_s$, the median being indicated by a bold horizontal line. Vertical lines characterise the lower and upper extreme of each distribution [22]. The mean lengths of sintered matrix particle segments are marked by bold dashed lines (Fig. 4-5). For mini-composite (MC) specimens, the mean length $l_s$ increases from 0.19 μm after one hour to 0.29 μm after 100 hours at 1300 °C. For bidirectional laminate (LAM) specimens, the increase in mean length $l_s$ is less pronounced, ranging from 0.14 μm after one hour to 0.19 μm after 50 hours and 0.21 μm after 100 hours at 1300 °C.

# 5. Discussion

The above results show that density measurements alone are not sufficient to characterise the densification behaviour of the porous CMC matrix. Generally, the embedded fibres are expected to affect matrix densification during high-temperature exposure [23, 24]. However, their exact role is not clear from the results shown in Fig. 4-1: the modest increase in the ratio of matrix bulk density to matrix skeletal density $\rho_m/\rho_{m_0}$ of the laminate specimens can be attributed to several factors, such as the presence of processing-induced macropores or crack-like defects, which tend to resist matrix

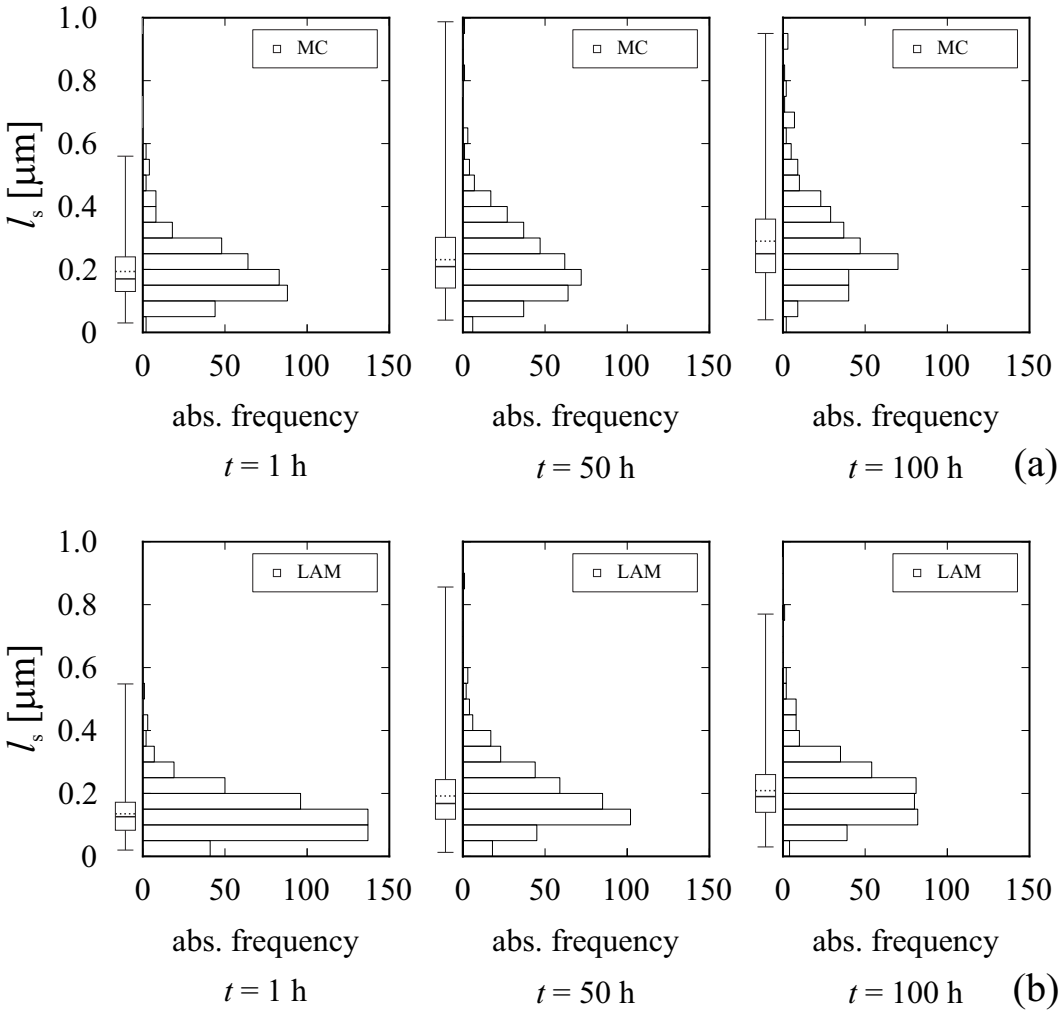


4-5 Histograms of the lengths $l_s$ of sintered particle segments for all five fibre cross-sections in mini-composite (a) and laminate specimens (b) after thermal exposure to 1300 °C for different times $t$.

densification [20]. Furthermore, as a result of the different unconstrained densification rates of the porous matrix and the embedded dense fibres, specimens with both uni- and bidirectional fibre orientation are subject to shrinkage-induced stresses. Tensile stresses in the porous matrix phase, in particular, might lead to the formation of additional matrix microcracks [25], which represent open pores during matrix density determination, effectively reducing the obtained matrix bulk density of the specimens. This may result in an underestimation of the increase in the ratio $\rho_m/\rho_{m_0}$ for specimens containing fibres.

Although the increase in matrix bulk density is modest and the inter-fibre matrix microstructure of mini-composites and laminate specimens, on cross-sectional images (Fig. 4-2), appears to be unaffected by the high-temperature exposure, microstructure evolution takes place, as qualitatively evidenced by the increase in mean length fractions of matrix particle segments sintered to the fibres. Fig. 4-5 indicates that the increase in length fractions of sintered particle segments is primarily due to an increase in the lengths of existing sintered particle segments.

Assuming that unidirectional fibre orientation imposes the least, and $\alpha = \pm 45°$ fibre orientation

constitutes the strongest constraint on matrix densification during high-temperature exposure, variations in matrix microstructure of actual all-oxide CMCs with $0° < \pm\alpha < 45°$ fibre orientation are supposed to be similar to those observed here.

# 6. Summary

This report recapitulates the effects of extended high-temperature exposure on the microstructure of all-oxide CMCs with porous matrix phase. Specimens with uni- and bidirectional fibre orientation, as well as reference matrix specimens, were thermally treated at a temperature of 1300 °C for up to 100 hours.

The specimens exhibit different degrees of matrix densification, as indicated by the increase in matrix bulk density with exposure time. The presence of matrix macropores and embedded fibres is expected to retard matrix densification. The mean length fractions of particle segments sintered to the fibre contour increases with exposure time, which can be attributed to an increase in sinter segment lengths.

The sintering mechanisms affecting microstructure evolution during high-temperature exposure are highly complex. Additional mechanical tests are required in order to evaluate the impact of the observed microstructural variations on the mechanical properties, particularly crack deflection ability and in-situ fibre strength, of all-oxide CMCs.

# Bibliography


[1] Evans AG, Zok FW (1994) The physics and mechanics of fibre-reinforced brittle matrix composites. J Mater Sci 29:3857–96

[2] Kerans RJ (1994) Issues in the control of fiber-matrix interface properties in ceramic composites. Scripta Metall Mater 31:1079–84

[3] Naslain RR (1998) The design of the fibre-matrix interfacial zone in ceramic matrix composites. Compos Part A 29:1145–55

[4] Evans AG, Marshall DB (1989) The mechanical behavior of ceramic matrix composites. Acta Metall 37:2567–83

[5] Okabe T, Komotori J, Shimizu M, Takeda N (1999) Mechanical behavior of SiC fiber reinforced brittle-matrix composites. J Mater Sci 34:3405–12

[6] Tu W-C, Lange FF, Evans AG (1996) Concept for a Damage-Tolerant Ceramic Composite with "Strong" Interfaces. J Am Ceram Soc 79:417–24

[7] Haslam JJ, Berroth KE, Lange FF (2000) Processing and properties of an all-oxide composite with a porous matrix. J Eur Ceram Soc 20:607–18

[8] Filipuzzi L, Camus G, Naslain R, Thebault J (1994) Oxidation Mechanisms and Kinetics of 1D-SiC/C/SiC Composite Materials: I, An Experimental Approach. J Am Ceram Soc 77:459–66

[9] Jacques S, Guette A, Langlais F, Naslain R (1997) C(B) materials as interphases in SiC/SiC model micro-composites. J Mater Sci 32:983–88

[10] Levi CG, Yang JY, Dalgleish BJ, Zok FW, Evans AG (1998) Processing and Performance of an All-Oxide Ceramic Composite. J Am Ceram Soc 81:2077–86

[11] Blanks KS, Kristoffersson A, Carlström E, Clegg WJ (1998) Crack Deflection in Ceramic Laminates Using Porous Interlayers. J Eur Ceram Soc 18:1945–51

[12] Mattoni MA, Yang JY, Levi CG, Zok FW (2001) Effects of Matrix Porosity on the Mechanical Properties of a Porous-Matrix, All-Oxide Ceramic Composite. J Am Ceram Soc 84:2594–602

[13] Kanka B, Schmücker M (2009) Long-Term High Temperature Stability of WHIPOX All-Oxide CMC. 33rd International Conference and Exposition on Advanced Ceramics and Composites (ICACC'09), Daytona Beach

[14] 3m Corporation (2004) Nextel™ Ceramic Textiles Technical Notebook. 3m Ceramic Textiles and Composites, St. Paul

[15] Kanka B, Luxem W, Schneider H (2001) Processing and microstructure of WHIPOX™. International Conference on High-Temperature Ceramic Matrix Composites (HT-CMC 4), Munich

[16] Kanka B (2011) Ceramic Fibre Composite Material. U.S. Patent 7,919,039. United States Patent and Trademark Office, Alexandria

[17] Sasol Germany GmbH (2007) PURAL®/CATAPAL® High purity aluminas. Sasol Germany GmbH, Hamburg

[18] Rasband WS (1997-2014) ImageJ Image Processing and Analysis. U. S. National Institutes of Health, Bethesda

[19] Nettleship I, McAfee RJ, Slaughter WS (2002) Evolution of the Grain Size Distribution during the Sintering of Alumina at 1350 °C. J Am Ceram Soc 85:1954–60

[20] De Jonghe LC, Rahaman N (2003) Sintering of Ceramics. In: Somiya S, Aldinger F, Claussen N, Spriggs RM, Uchino K, Koumoto K, Kaneno M (eds) Handbook of Advanced Ceramics, 1st edn. Academic Press, Oxford, pp. 187–264

[21] Schmücker M, Mechnich P (2008) Microstructural coarsening of Nextel™ 610 fibers embedded in alumina-based matrices. J Am Ceram Soc 91:1306–08

[22] McGill R, Tukey JW, Larsen WA (1978) Variations of Box Plots. Am Stat 32:12–6

[23] Lam DCC, Lange FF (1994) Microstructural Observations on Constrained Densification of Alumina Powder Containing a Periodic Array of Sapphire Fibers. J Am Ceram Soc 77:1976–78

[24] Scherer GW (1987) Sintering with Rigid Inclusions. J Am Ceram Soc 70:719–25

[25] Evans AG (1982) Considerations of Inhomogeneity Effects in Sintering. J Am Ceram Soc 65:497–501